Self-generation of Magnetic Fields in Discontinuous Plasmas

Frank Modica[1], Tomasz Plewa[1], Andrey Zhiglo[2]
(1) Florida State University
(2) Kharkov Institute of Physics and Technology, Kharkov, Ukraine

Introduction

Hydrodynamic instabilities play an important role in the evolution of astrophysical systems. The Rayleigh-Taylor instability (RTI), for example, occurs when a dense fluid is accelerated against a light fluid, producing well known finger-like structures and material mixing. In the case of supernova (SN) explosions, RTI occurs when a blast wave moves through materials of varying densities, such as layers of hydrogen and helium. Scientists have attempted to investigate this system experimentally in a laboratory setting. In our supernova Rayleigh-Taylor mixing experiment on the Omega laser [1], the instability is created using a laser to irradiate a target and drive a blast wave. The target is designed to mimic the H/He interface in a core-collapse supernova progenitor envelope. The experimental results differed from simulation outcomes, most notably by revealing suppressed RT mushroom-cap formation and significantly more extended RT spikes (see Fig. 1).

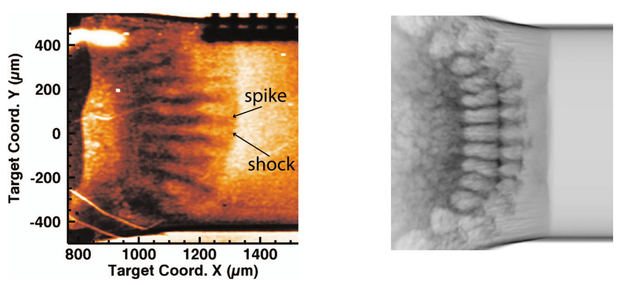

Figure 1 : (left panel) An x-ray radiographic image of an experiment that used a 3D, single-mode perturbation as the initial condition. (right panel) The results from a 3D FLASH simulation with 3D, single-mode initial conditions. Both images are at t=21 ns. [1]

The main goal of this work is to study the effects of magnetic fields and thermal conductivity on fluid flow instabilities, in particular the Rayleigh-Taylor instability. It is known that a misalignment of temperature and electron density gradients can generate a magnetic field from zero-field initial conditions (the Biermann battery effect).

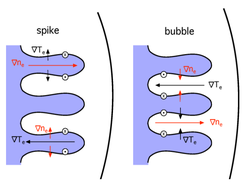

Figure 2 : The Biermann battery mechanism at the RT-unstable interface. The magnetic field is generated at the interface due to misalignment of gradients of electron number density and electron temperature. [1]

This field can then be modified due to complex interactions between ions and electrons in the plasma. Magnetic field and thermal conductivity are known to modify RTI growth and thus may account for the observed differences between computer models and experimental results. To this end, we implemented and verified generalized Ohm's law and anisotropic thermal conduction using the Braginskii formulation in the FLASH-based Proteus code. We present verification results of our implementation and preliminary results in application to the RTI problem under high-energy density conditions.

Computational Model

An electrically conducting fluid can be described using either a one-fluid or two-fluid model. In a one-fluid model, Maxwell's equations of electromagnetism are coupled with fluid equations via Ohm's Law. This model is usually considered accurate on short time scales where non-ideal effects are negligible. In a two-fluid model, the electrons and ions can be described individually by, for example, the Braginskii equations. [2] This is a more accurate description of the plasma, but requires a two-fluid code to solve twice as many equations for the density, momentum, and energy of each fluid, in addition to the magnetic field induction equation. Here we are using a single-fluid code to numerically solve the magnetohydrodynamic (MHD) equations in conservation form. Extended terms that we have implemented in our modified version of the FLASH code, Proteus, for anisotropic thermal conduction and magnetic field generation are in red boxes:

$$\frac{\partial \rho}{\partial t} + \nabla \cdot (\rho \mathbf{u}) = 0$$

$$\frac{\partial \rho \mathbf{u}}{\partial t} + \nabla \cdot \left(\rho \mathbf{u}\mathbf{u} - \frac{\mathbf{B}\mathbf{B}}{4\pi} \right) + \nabla P = \rho g$$

$$\frac{\partial \rho E}{\partial t} + \nabla \cdot \left[(\rho E + P)\mathbf{u} - \frac{\mathbf{B}\mathbf{B}}{4\pi} \cdot \mathbf{u} \right] = \rho \mathbf{u} \cdot g + \nabla \cdot (\kappa \cdot \nabla T) + Q$$

$$\frac{\partial \mathbf{B}}{\partial t} + \nabla \cdot (\mathbf{u}\mathbf{B} - \mathbf{B}\mathbf{u}) = \frac{c}{e}\left[\nabla \times \frac{\nabla P_e}{n_e} - \nabla \times \frac{(\nabla \times \mathbf{B}) \times \mathbf{B}}{4\pi n_e} - \nabla \times \frac{\mathbf{R}_T + \mathbf{R}_u}{n_e} \right]$$

In these equations, ρ is the fluid density, $\mathbf{u}$ is the velocity, $\mathbf{B}$ is the magnetic field, P is the fluid pressure, g is the gravitational constant, E is the total fluid energy, n_e is the electron density, P_e is the electron pressure, and Q, κ, $\mathbf{R_T}$ and $\mathbf{R_u}$ are the heat deposition source term, thermal conductivity tensor, thermal force, and friction force between ions and electrons, respectively, formulated according to [2].

We have attempted to bridge the gap between the one and two-fluid models using various strategies. In order to calculate n_e, we need to know the average ionization of the fluid. We obtained this by implementing the Thomas-Fermi equation of state. This allowed calculation of κ, P_e, and $\mathbf{R}_T$. $\mathbf{R}_u$ required knowledge of the relative velocity between ions and electrons, which was computed as $-\frac{c}{4\pi e n_e}\nabla \times \mathbf{B}$, an approximation valid in one-fluid models. It should be mentioned that we are assuming that the electrons and ions are in thermal equilibrium.

Verification Tests

A number of test simulations were done to verify that our magnetic field generation and anisotropic heat conduction modules were working properly. The first test is for the Biermann battery term introduced in Toth et al. [2] Given the following initial conditions:

$$\mathbf{B} = 0, \mathbf{u} = 0, n_e = n_0 + n_1 \cos(k_x x), p_e = p_0 + p_1 \cos(k_y y),$$

$$k_x = k_y = \frac{\pi}{10}, n_0 = p_0 = 1, n_1 = p_1 = 0.1$$

The exact solution for the rate of magnetic field generation is:

$$\frac{\partial B_z}{\partial t} = -\frac{k_x k_y n_1 p_1 \sin(k_x x)\sin(k_y y)}{\left[n_o + n_1 \cos(k_x x)\right]^2}$$

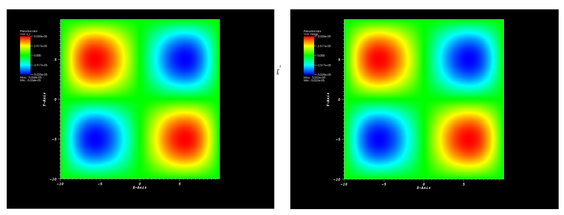

Figure 3 : (left panel) Numerical solution of the generated magnetic field source term, $\frac{\partial B_z}{\partial t}$, on a 100 x 100 grid. (right panel) Exact solution. Time t = 0.05 s.

Since it is known that magnetic field generation via the Biermann battery term depends on the orientation of temperature and electron number density gradients, we constructed a test which shows the results of all possible initial conditions simultaneously. In the image below, the domain extends from $0 \leq x \leq 360$, $0 \leq y \leq 360$. The orientation of the electron number density gradient (not shown) varies from 0 to 360 degrees with the x-axis, while the orientation of the temperature gradient (not shown) varies from 0 to 360 degrees with the y axis, where 0 degrees corresponds to a gradient in the direction of the x-axis. The magnitude of the temperature gradient increases with the z-axis. The generated magnetic field (shown) reaches a maximum when the two gradients are misaligned, and is zero when they are aligned, as expected.

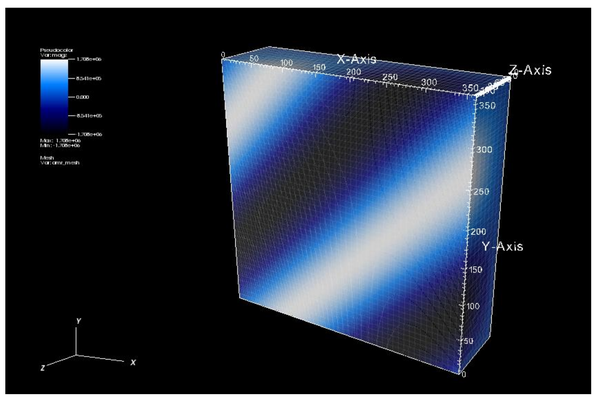

Figure 4 : Magnetic field generation source term, $\frac{\partial B_z}{\partial t}$, as a function of electron number density and temperature gradient orientation.

We tested our anisotropic thermal conduction module by initializing a circular magnetic field with the following initial conditions for temperature given by Parrish & Stone [3]:

$$T(r,\theta) = \left\{ \begin{array}{l} 12 \text{ if } (0.5 \leq r \leq 0.7) \text{ and } \left(\frac{11}{12} \leq \theta \leq \frac{13}{12}\right) \\ 10 \text{ otherwise} \end{array} \right\}$$

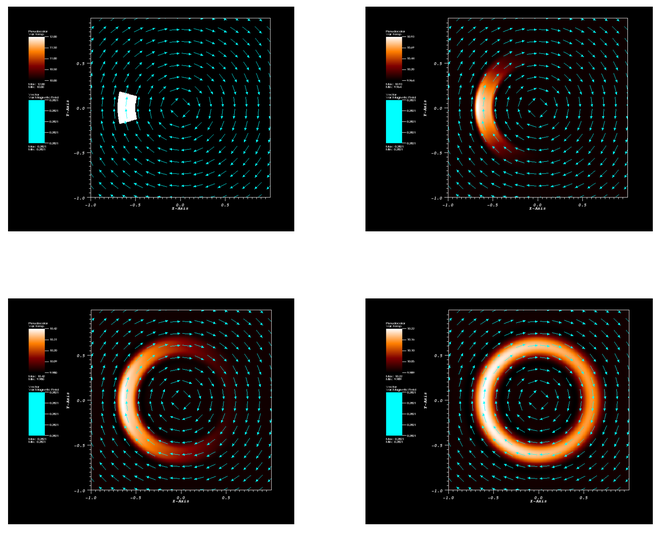

Figure 5 : Results of the Parrish & Stone anisotropic thermal conduction verification test on a 400 x 400 grid. The temperature distribution is shown at times t = 0, 10, 50, and 200. Heat flows along magnetic field lines, as expected.

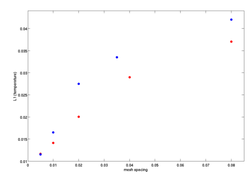

Figure 6 : Convergence of the L1 error norm of temperature as a function of the mesh resolution for the Parrish & Stone test problem. Our results are shown in red, and those of Parrish & Stone are shown in blue.

Results

Below we show preliminary results of RTI simulations incorporating our new physics modules.

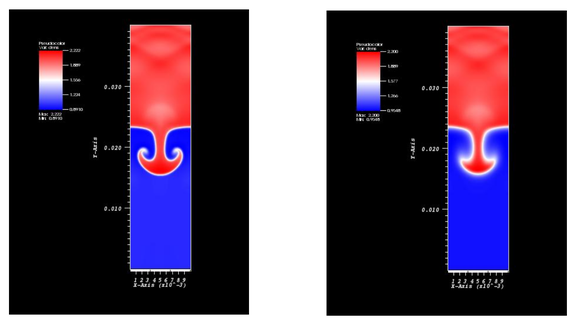

Figure 7 : (left panel) A pure hydro simulation of RTI. (right panel) Hydro with anisotropic thermal conduction and magnetic field generation. We see less structure with the additional physics, which may help explain the relatively featureless fingers in the experiment. [1] All results are at time t = 20 ns on a 64 x 256 grid.

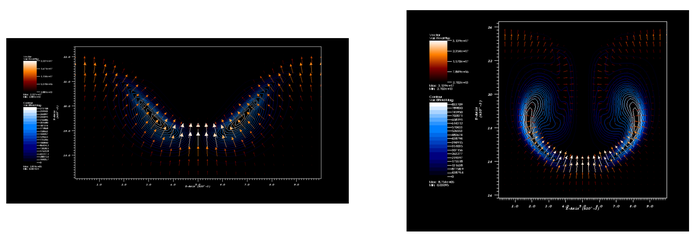

Figure 8 : Heat fluxes and magnetic field generation at the RT-unstable interface at time t = 6.7 ns and 20 ns, on a 64 x 256 grid.

Future Work

Our ultimate goal is to complete our physics model so that we can obtain a better understanding of RTI in these high-energy density conditions. A natural next step to having a full Braginskii model of RTI would be to implement viscosity. Given the great deal of physics capabilities added to our code, additional verification and validation tests are also necessary. New solution techniques may also prove to be useful. For example, an implicit solver for thermal conduction would enable studies of more extreme, diffusion-dominated situations. (In such cases, the time step is often a performance bottleneck.)

References

[1] Kuranz, C. C., Drake, R. P., & Grosskopf, M. J., et al. 2010, Phys. Plasmas, 17, 052709
[2] Braginskii, S. I., in Review of Plasma Physics (translated from Russian), ed. M.A. Leontovich, Consultants Bureau, New York, 1965, Vol. 1, 205
[3] Tóth, G., van der Holst, B., & Sokolov, I. V., et al. 2012, J. Comput. Phys., 231, 870
[4] Parish, I. J., & Stone, J. M. 2005, ApJS, 633, 334